Room-temperature H_2 splitting and N_2-hydrogenation induced by a neutral Lu^{II} complex

Evangelos Papangelis,[a#] Luca Demonti,[a#] Iker del Rosal,[b] Angus Shephard,[a] Laurent Maron,[b]* Grégory Nocton[a]* and Thomas Simler[a]*

a) LCM, CNRS, Ecole polytechnique, Institut Polytechnique de Paris, Route de Saclay, 91120 Palaiseau, France.
E-mail: thomas.simler@polytechnique.edu; gregory.nocton@polytechnique.edu

b) LPCNO, UMR 5215, Université de Toulouse-CNRS, INSA, UPS, Toulouse, France.
E-mail: laurent.maron@irsamc.ups-tlse.fr

# These authors contributed equally

Abstract

The direct splitting of the H_2 and N_2 molecules are challenging reactions that are closely related to the Haber–Bosch ammonia synthesis process. Until now, such reactivity has never been observed in the case of molecular lanthanide species. Here, we show that careful selection of the ligand scaffold allows the isolation and characterization of a kinetically stable but highly reactive Lu^{II} complex. This divalent lanthanide species enables direct H_2 splitting at room temperature, an unknown reactivity in lanthanide chemistry, which has been fully corroborated by DFT calculations. In addition, the Lu^{II} complex readily binds N_2, leading to an end-on coordinated diazenido $(N_2)^{2-}$ lanthanide complex. The latter can be hydrogenated under very smooth conditions (*ca*. 1.2 bar H_2, ambient temperature) to form a unique Lu^{III}–NH_2 complex. Direct N_2 hydrogenation and cleavage are thus accessible using low-valent molecular rare-earth metal complexes.

Introduction

The question of dihydrogen, how it is produced, and how it is used is central to sustainability issues and the decarbonization of the industry.[1] The reversibility of catalytic hydrogenation and dehydrogenation processes is at the heart of this question, as is the transport of H_2 by liquid organic carriers (LOHC).[2] This is particularly true in research on Sustainable Aviation Fuels (SAF) and shipping. Ammonia has been proposed as a desirable hydrogen carrier for the latter because of its hydrogen density and also as a direct fuel.[3] Still, direct ammonia combustion poses the question of N_2O formation, a potent greenhouse gas.[4] Catalytic processes that combine the cleavage of H_2 and selective transfer to nitrogen are desirable. Using low-cost heterogeneous catalytic systems, the Haber–Bosch process is currently the most efficient industrial process for producing ammonia by nitrogen hydrogenation.[5] While it is

difficult to question the massive production of ammonia *via* this process, smaller-scale units in less industrial environments, where H_2 is produced from green methods, could make way for catalysts capable of generating ammonia at lower energy costs and with greater versatility.[3] Developing processes that can split the H_2 molecule and selectively functionalize simple substrates, such as nitrogen (for ammonia)[6] or CO_2 (for formic acid or methanol),[7] remains a major challenge in modern organometallic chemistry.

Homogeneous pathways for converting N_2 to NH_3 have been made recently, principally with transition metals and uranium.[8] From a mechanistic point of view, the conversion of N_2 and H_2 to ammonia involves different possible scenarios. In the first one, H_2 cleavage occurs first, forming hydride species, which then transfer the hydrogen atoms to dinitrogen. In the second one, N_2 cleavage occurs first, and the resulting nitride is hydrogenated. In the last scenario, synergetic hydrogenation of a reduced N_2 ligand occurs. Among these possibilities, the role of multi-metallic hydride species in the hydrogen atom transfer to dinitrogen has been documented by Hou and co-workers.[9] Hydrogenation of bridged nitrido units, formed after cleavage of dinitrogen, has been recently reported by the groups of Walter and Zhu.[8d,10] It is noteworthy that the direct hydrogenation of reduced dinitrogen adducts has been only described with an organometallic Zr complex.[6b]

In the case of rare-earth (RE) elements, which are constituted by the lanthanides along with the closely related Y and Sc, very rare examples of N_2 functionalization have been disclosed. Corresponding complexes have been obtained by reaction of complexes bearing side-on triply-reduced $(N_2)^{3-}$ ligands with electrophiles or proton donors (Figure 1a),[11] but direct reaction with H_2 has not been witnessed to date. Recently, Arnold and co-workers showed that dinuclear Sm and Ce complexes could generate bis- and tris(silyl)amine with a turnover of up to 4 using a large excess of metallic reductant in the presence of excess Me_3SiCl or proton sources.[12] Additionally, following seminal reports on photochemical assistance in producing ammonia from N_2,[13] the group of Borbas recently reported photocatalytic ammonia formation by a Sm complex bearing a built-in coumarin chromophore.[14]

Historically, the chemistry of divalent lanthanide complexes has been dominated by Sm^{II}, Eu^{II}, and Yb^{II} species, which feature relatively stable $4f^n$ Ln^{II} electronic configurations.[15] The corresponding metallocene chemistry has flourished, especially in the context of single-electron transfer (SET) reductions, typically leading to Ln^{III} end products.[16] Although cyclopentadienyl (Cp) complexes of all the lanthanides, except radioactive Pr, have been isolated in the +II oxidation state,[17] fewer studies have focused on the so-called "non-classical divalent lanthanides",[18] consisting of the remainder of the 4f series. This relative scarcity can be traced back to experimental difficulties in handling these very reactive and reducing species.[19] Among them, Tm^{II} is the most accessible in terms of reduction potential, yet displays strong reducing properties beneficial for molecular activation *via* SET reactions.[11d,20]

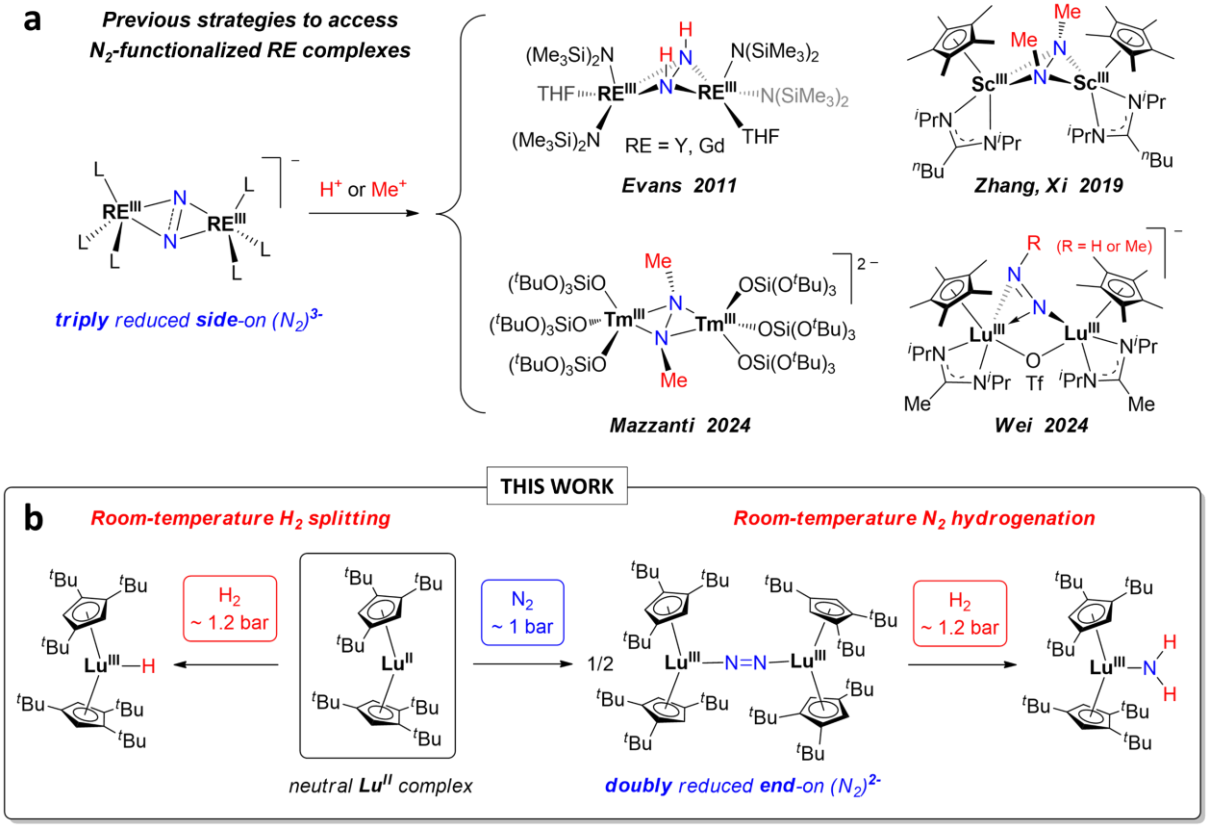

Figure 1. (a) Previous strategies to access N_2-functionalized rare-earth metal complexes. (b) Reactivity described in this work.

In this context, our group recently showed that the Tm^{II} complex $[Tm(Cp^{ttt})_2]$ (Cp^{ttt} = 1,2,4-tris(*tert*-butyl)cyclopentadienyl) displays unique reactivity in terms of CO reductive coupling and subsequent functionalization reactions.[21] The choice of the Cp^{ttt} ligand was crucial to kinetically stabilize the reactive metal center while still allowing the coordination of an exogenous ligand.[22] The three bulky *tert*-butyl substituents confer high thermal stability but slightly hamper reactivity, as $[Tm(Cp^{ttt})_2]$ does not react with N_2, contrary to the less sterically protected analogues.[20a,23] An extreme case of stabilization was recently reported by Long, Harvey and co-workers through the use of the penta-substituted Cp^{iPr5} (Cp^{iPr5} = pentaisopropylcyclopentadienyl) ligand. The redox potential of the corresponding Tm^{II} complex was evaluated as high as –1.57 V, more than 1 V less reducing than other Tm^{II} Cp-type complexes.[19,21]

In the present study, we were interested in investigating whether the Cp^{ttt} ligand would allow the stabilization of even more reducing Lu^{II} complexes. In addition to advantageous properties in terms of quantum applications,[24] Lu^{II} species appear particularly attractive to uncover novel reactivities, especially in terms of small molecule activation *via* SET reductions. Unlike Tm^{III} species that are strongly paramagnetic, Lu^{III} end products are diamagnetic, allowing precise monitoring of reactions by multinuclear NMR spectroscopy. Surprisingly, only three molecular Lu^{II} complexes have been reported to date (Figure 2), the two separated ion-pair complexes $[K(crypt)][LuCp'_3]$ (Cp' = $C_5H_4SiMe_3$)[25] and

[K(crypt)][Lu(OAr*)$_3$] (OAr* = 2,6-bis(adamantly)-4-^{t}Bu-C$_6$H$_2$O),[24,26] and the neutral [Lu(Cp^{iPr5})$_2$] complex.[17d]

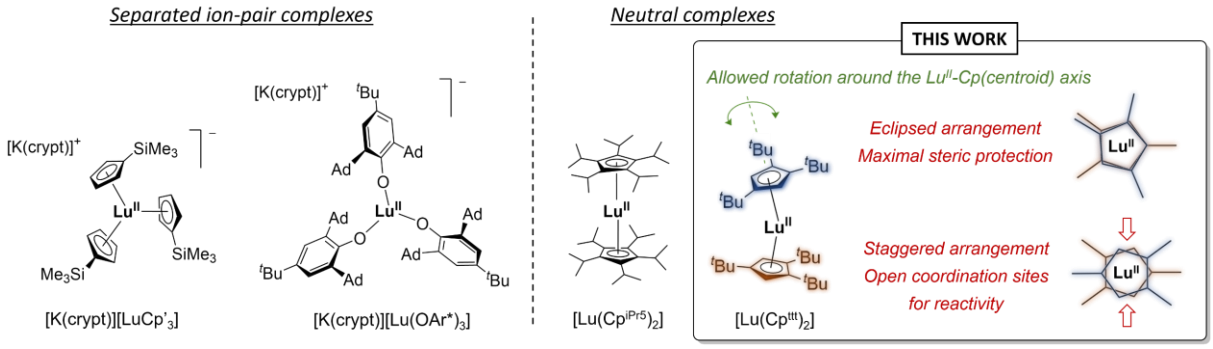

Figure 2. Structures of the previously reported Lu^{II} complexes and comparison with this work. The fluxional behavior of the Cp^{ttt} ligand allows the formation of two possible arrangements: the eclipsed arrangement offers maximal steric protection for the metal center and enhanced kinetic stability while the staggered arrangement provides available coordination sites for SET reactivity.

In this work, we show how the fluxional behavior of the Cp^{ttt} ligand in [Lu(Cp^{ttt})$_2$] allows the stabilization of a highly reactive Lu^{II} complex while still offering an open coordination site for original reactivity (Figure 2). It is worth noting that, during this work, Evans and co-workers reported the synthesis of the related [Sc(Cp^{ttt})$_2$] and its coordination chemistry towards CO and isocyanides.[27] Herein, we show that [Lu(Cp^{ttt})$_2$] induces unprecedented reactivities in lanthanide chemistry, such as direct H_2 splitting and N_2 hydrogenation under very smooth conditions (Figure 1b).

Results and discussion

Synthesis and characterization of [Lu(Cp^{ttt})$_2$]

The parent Lu^{III} complex, [Lu(Cp^{ttt})$_2$(BH$_4$)] (**1**), was prepared by a salt metathesis reaction between KCp^{ttt} and [Lu(BH$_4$)$_3$(THF)$_3$],[28] using a procedure similar to that described for the synthesis of [Ln(Cp^{ttt})$_2$(BH$_4$)] (Ln = Tm, Dy),[20c,29] and isolated in a 39% crystalline yield. In contrast to the preparation of other [Ln(Cp^{ttt})$_2$(BH$_4$)] complexes,[20c,29-30] longer reaction times were necessary to achieve reasonable conversion into **1**. The latter was isolated in a 39% yield upon crystallization from pentane at –40 °C. The mother liquor, which was found to be composed of **1** along with the corresponding half-sandwich complex [Lu(Cp^{ttt})(BH$_4$)$_2$(THF)],[31] can be conveniently reused in subsequent synthesis batches of **1** to improve the yield. As lutetium is the last member in the 4f series, its ionic radius may explain the increased difficulty in accommodating two bulky Cp^{ttt} ligands around the metal center.

The X-ray structure of **1** (Figure 3b) confirmed the coordination of two η^5-Cp^{ttt} and one κ^2-bound borohydride to the Lu^{III} center. In comparison with the isomorphous Tm^{III} complex,[20c] the Lu–Cp(ctr) (ctr = ring centroid) separation is slightly shorter (2.322 Å for Lu *vs.* 2.356 Å for Tm), in

agreement with the smaller ionic radius of Lu.[32] The ^{1}H NMR spectrum of **1** displays three resonances for the coordinated Cp^{ttt} ligands, consistent with an overall C_{2v} symmetric species in solution. One notable feature in the IR spectrum of **1** is the presence of three moderately intense bands in the region 2000–2500 cm^{-1}, more precisely one doublet band at 2459 and 2413 cm^{-1} associated with one additional band at 2112 cm^{-1}, arising from the terminal κ^2-bound BH_4.[33] These bands are blue-shifted by *ca.* 50 cm^{-1} with respect to those in $[LuCp_2(BH_4)(THF)]$ initially reported by Schumann and co-workers.[34]

To access $[Lu(Cp^{ttt})_2]$ (**2**), reduction of **1** was performed by treatment with excess KC_8 in pentane at room temperature under an argon atmosphere for 5 days (Figure 3a). As **2** is extremely sensitive towards N_2, special precautions must be taken to avoid adventitious reaction with traces of N_2, even when working in an argon-filled glovebox (see Supplementary Information for details). It should be noted that previous reports on the attempted isolation of non-classical divalent lanthanide $[Ln(Cp^{ttt})_2]$ complexes highlighted the difficulty in isolating these species owing to their high reactivity and solubility.[35]

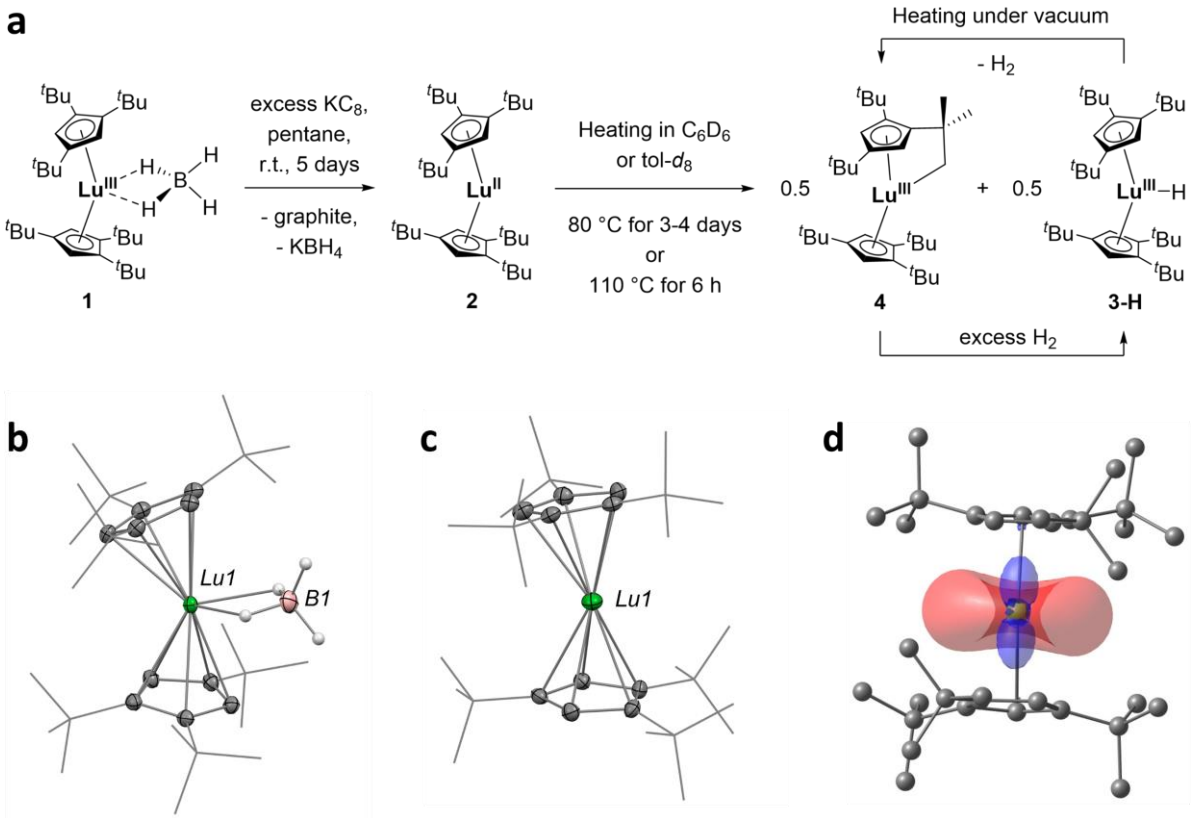

Figure 3. (a) Synthesis and thermolysis reactivity of **2**. (b) Molecular structures of **1** and (c) of one of the two independent molecules of **2** in the solid state (see also Figure S37). The thermal ellipsoids are at the 40% probability level, except for the ^{t}Bu groups depicted in wireframe, and H atoms have been omitted for clarity, except those on the borohydride unit. (d) SOMO of **2** consisting of the Lu d_{z^2} orbital.

Building on our recent success in crystallizing the related Tm^{II} complex $[Tm(Cp^{ttt})_2]$,[21] orange-red crystals of **2** suitable for X-ray diffraction (XRD) studies were isolated in 18% yield after crystallization from pentane at low temperature (–40 °C). Although the isolated crystalline yield is relatively low, which can be traced back to the very high solubility of **2** in hydrocarbon solvents, the mother liquor was found to be composed of **2** along with variable amounts of clean thermolysis products (see below), as evidenced by ^{1}H NMR analysis.

The molecular structure of **2** in the solid state (Figure 3c) displays two independent molecules of **2** in the asymmetric unit, featuring very similar metric data, and confirms the formation of a base-free bent metallocene complex. The two Cp^{ttt} ligands are in an eclipsed arrangement, providing efficient kinetic stabilization of the Lu^{II} metal center. A comparison of the steric shielding in **2** *vs.* that in $[Lu(Cp^{iPr5})_2]$[17d] by the Guzei method[36] (see Supporting Information for details) revealed very similar *G* values (83.5 and 85.5%, respectively). The bent arrangement in **2**, which displays an average Cp(ctr)–Lu–Cp(ctr) (ctr = ring centroid) angle of 167.2°, is typical for Cp-based Ln^{II} sandwich complexes.[16] Linear coordination has only been observed when using the Cp^{iPr5} ligand, which presents a higher symmetry and different steric profile than the Cp^{ttt} ligand.[17d] In contrast to the previously reported $[Ln(Cp^{ttt})_2]$ (Ln = Sm, Eu, Yb, Tm) complexes, for which a monotonic contraction in the Ln–Cp(ctr) separation of *ca.* 0.018 Å is observed per atomic number increment, the average Lu–Cp(ctr) distance of 2.305 Å in **2** does not follow this trend (Figure S41). Although there have been discussions regarding the model that should be best used to fit the variation in bond distances due to the lanthanide contraction,[37] the Lu–Cp(ctr) in **2** appears *ca.* 0.056 Å shorter as would be expected from a simple linear fit. The apparent decrease in ionic radius can be traced back to the $4f^n5d^1$ (n = 14) configuration for Lu^{II}, compared to the $4f^{n+1}$ configuration adopted by the divalent Sm, Eu, Yb and Tm congeners, and covalent interactions involving the populated 5d orbital.[25,38]

The ^{1}H NMR spectrum of **2** at room temperature displays two hardly identifiable broad resonances. Upon heating to 80 °C, a better-resolved spectrum can be obtained with two main resonances at δ 2.0 ($\Delta\nu_{1/2} \approx 70$ Hz) and 0.9 ppm ($\Delta\nu_{1/2} \approx 200$ Hz) in a respective 1:2 ratio, corresponding to the ^{t}Bu groups of freely rotating Cp^{ttt} ligands.[39] Continuous-wave X-band EPR measurements performed on a solution of **2** in pentane at room temperature only revealed one broad isotropic signal at g = 2.274 with unresolved hyperfine coupling, which disappeared upon addition of N_2 (Figures S34–35). In contrast, an eight-line EPR pattern was reported for $[K(crypt)][LuCp'_3]$ (^{175}Lu, I = 7/2, 97.4% natural abundance),[25] whereas $[Lu(Cp^{iPr5})_2]$ did not give rise to an observable signal.[17d] The geometry of complex **2** was optimized at the DFT level (B3W91 functional) and the optimized geometry compares well with the experimental one. In particular, the Lu–Cp(ctr) distance is well reproduced (2.335 *vs.* 2.305 Å experimentally) as well as the Cp(ctr)–Lu–Cp(ctr) angle (166.6° *vs.* 167.2° experimentally). The SOMO (Figure 3d) of **2** appears to be the metal d_{z^2} orbital, in line with a Lu^{II} $4f^{14}5d^1$ configuration, and agrees with the isotropic g value of the EPR signal.

The UV–vis spectrum of **2** in pentane (Figure 4) shows a major absorption band at 435 nm (ε = 2800 $L \cdot mol^{-1} \cdot cm^{-1}$), along with the onset of a strong band below 350 nm. It contrasts with the spectrum of the related neutral $[Lu(Cp^{iPr5})_2]$ complex, which features minimal absorption in the visible region.[17d] In comparison, in the $[K(crypt)][LuCp'_3]$ separated ion-pair complex, an intense band was observed at 518 nm and assigned to a metal–to–ligand charge-transfer (MLCT) transition.[25] TDDFT calculations were carried out in *n*-pentane to obtain the UV–vis spectrum of **2** (Figure S42). An absorption band is found around 400 nm, in agreement with the experimental spectrum, and consists of an MLCT excitation from the SOMO (d_{z^2}) to the Lu–Cp^{ttt} antibonding orbital.

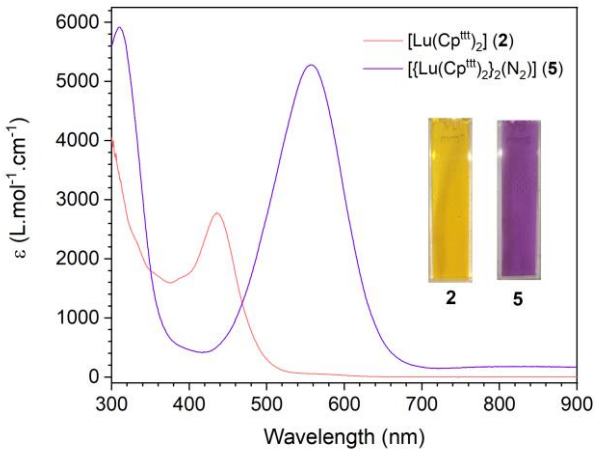

Figure 4. Room temperature UV–vis–NIR absorption spectra in pentane of **2** (C = 4.5 mM) and *in situ* formed **5** (C = 0.8 mM) and photograph of the cuvettes.

*Thermolysis reactivity of **2***

The thermal stability of **2** was investigated at different concentrations by ^1H NMR and UV–vis spectroscopy. For a dilute solution of **2** in pentane (C = 4.5 mM), a decrease in intensity of *ca.* 6% was observed in the UV-vis spectrum for the most intense absorption band at 435 nm over 2 h (Figure S32). More concentrated solutions were found to be more stable over time as the ^1H NMR spectrum of **2** in C_6D_6 (C = 30–50 mM) revealed no significant formation of thermolysis products over several days. The thermal stability of Lu^{II} complexes appears to be highly dependent on the ligand environment: at room temperature and in hydrocarbon solvents, $[K(crypt)][LuCp'_3]$ features a half-life of *ca.* 20 min,[25] whereas $[K(crypt)][Lu(OAr^*)_3]$ slowly decomposes over the course of several days.[24,26] An exceptional thermal stability was reported for $[Lu(Cp^{iPr5})_2]$, synthesized upon extensive heating at elevated temperatures (160–180 °C).[17d]

Heating a solution of **2** in C_6D_6 at 80 °C for several days led to an unexpectedly clean and well-defined ^1H NMR spectrum, showing the formation of the Lu^{III} hydride complex **3-H** and the cyclometallated complex **4** (Figure 3a) in close to equimolar amounts (see Figures S8–10). The identity of **4** was testified by its reactivity towards hydrogenolysis, as complete and immediate conversion into

3-H occurred upon addition of H_2 (Figure S9). A similar hydrogenolysis reactivity had been earlier reported by Andersen and co-workers on the cerium analogue of **4**.[40] The ^{1}H NMR spectrum of **4** displays, notably, two doublets at δ 0.65 and –0.18 ppm, with a $^2J_{HH}$ coupling constant of 13.5 Hz, for the diastereotopic protons of the cyclometallated methylene group. The characterization data of **3-H** will be discussed in detail in the next section. The hydrogenolysis reaction is reversible as heating a degassed solution of **3-H** under static vacuum for several days led to complete conversion back to **4** (Figures S11–12). The formation of **4** and its reactivity with H_2 to form **3-H** were also investigated computationally. The formation of **4** implies a bimetallic transition state (TS) on the triplet spin potential energy surface (PES) where the hydrogen from one ^{t}Bu group of one molecule of **2** is transferred to the Lu center of a second molecule of **2** (Figure S43). The associated barrier is 39.0 kcal·mol^{-1}, in line with the relative stability of **2** at room temperature and the experimental observation of a slow thermal degradation at 80 °C. Yet, the reaction is exothermic by 20.8 kcal·mol^{-1} due to the formation of one equivalent of **4** and one of **3-H**. The hydrogenolysis of complex **4** to form **3-H** (Figure S44) is both kinetically (barrier of 7.2 kcal·mol^{-1}) and thermodynamically favorable (–15.8 kcal·mol^{-1}). The activation barrier of 22.9 kcal·mol^{-1} for the reverse transformation is fully consistent with the dehydrogenation of **3-H** into **4** accessible upon heating.

*Reactivity of **2** towards small molecules: H_2 splitting*

The clean access to **2** as a rare base-free, room-temperature stable and highly soluble divalent lanthanide complex gave us the opportunity to study its reactivity towards industrially relevant small molecules, such as H_2, which usually does not bind strongly with f-elements. Herein, its coordination to the lanthanide center in **2** would not suffer from the presence of a better ligand.[41] Due to its unique properties, **2** reacts with H_2 under very smooth conditions (1.2–1.5 bar of H_2, ambient temperature), leading to quantitative conversion into the hydride complex **3-H** over the course of 1–3 days (Figure 5a). Reaction with D_2 proceeded similarly, yielding the Lu^{III} deuteride **3-D**, without any appreciable deuteration of the ligand backbone.[40] It should be stressed that the reactivity of **2** with H_2 is much faster than its thermal decomposition into **3-H** and **4** (see Figure S32), meaning that another direct pathway must be active to form **3-H** (see below for mechanistic insights by DFT calculations).

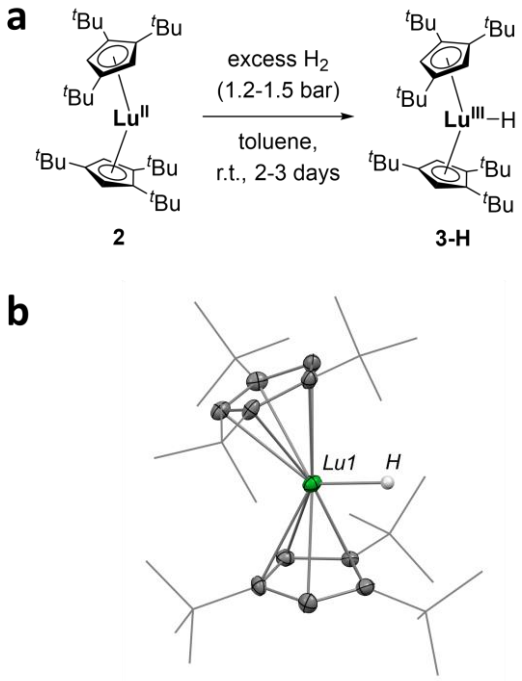

Figure 5. (a) Synthesis of **3-H** by reaction of **2** with H_2. (b) Molecular structure of **3-H** in the solid state with thermal ellipsoids at the 40% probability level (except for the ^{t}Bu groups depicted in wireframe). H atoms, except for the lutetium H atom, have been omitted for clarity.

In the ^{1}H NMR spectrum of **3-H**, the hydride resonance is detected as a downfield singlet at δ 10.3 ppm while the aromatic Cp^{ttt} protons give rise to a singlet at δ 6.13 ppm. Unrestricted rotation of the Cp^{ttt} ligands leads to an overall C_{2v} symmetry in solution, as evidenced by the presence of two singlets for the ^{t}Bu groups in a 2:1 ratio.[39a] In the IR spectrum of **3-H**, the Lu–H stretching frequency could not be identified, even upon direct comparison with the spectrum of **3-D**, similarly to what was also reported for the Ce analogue $[Ce(Cp^{ttt})_2H]$.[40] The molecular structures of **3-H** and **3-D** were unambiguously established by single-crystal XRD analyses, confirming the formation of rare examples of monomeric Ln^{III} complexes bearing terminal hydride or deuteride ligands (Figure 5b and Figure S39).[42] Although the H and D atoms on lutetium were located on the electron density map, the Lu–H/D separations (1.73(8) and 1.81(5) Å, respectively) suffer from low precision and may not be fully representative of the actual bond distances. They appear particularly short compared to the lutetium-hydride distances in related Cp-type complexes.[43] The Lu–Cp(ctr) distances in **3-H/D** are identical, within experimental error, to those in **2**, whereas the presence of the hydride leads to a more acute Cp(ctr)–Lu–Cp(ctr) angle (in average 167.2° in **2** *vs.* 153.1° in **3-H**), *i.e.* a larger deviation from linearity.

To the best of our knowledge, direct H_2 splitting by molecular lanthanide complexes is unprecedented to date. This strategy offers a novel route for the synthesis of molecular Ln^{III}–H species, typically obtained by hydrogenolysis of Ln–alkyl bonds.[33b,42,44] It can be noted that, in rare instances, molecular RE hydrides have been obtained upon treatment of trivalent complexes with strong alkali metal reductants.[43a,45] However, such reactions did not involve H_2 activation but rather undefined

hydrogen abstraction from solvents or possible aromatic C–H activation.[45e] Although elemental zerovalent lanthanides are known to react with hydrogen at elevated temperatures to afford binary Ln hydrides, no such reaction has been observed with molecular Ln species.[33b,42] Weak coordination of H_2 to a lanthanide complex has only been spectroscopically evidenced for the base-free Eu^{II} complex $[Eu(C_5Me_5)_2]$, in which case no metal oxidation and formation of a hydride complex occurred.[46] Very recently, this phenomenon has been extended to 5f elements with spectroscopic and computational evidence of the reversible formation of a U^{III}–H_2 complex.[47] Regarding heterogeneous lanthanide systems, nondissociative dihydrogen binding has also been very recently evidenced by solid-state NMR studies under pressure of H_2.[48] Finally, it is worth noting that, within the actinide series, some U^{II} and Th^{II} complexes were reported to activate H_2, leading to higher-valent hydride complexes, but the corresponding mechanisms remain elusive.[49]

DFT calculations were performed to shed light on the mechanism of the unusual H_2 activation reactivity of **2**. Reaction profiles were calculated on the triplet and singlet Potential Energy Surface (PES) (Figure S45), and the most probable profile is discussed (Figure 6a). The reaction begins with the formation of a weak van der Waals adduct of H_2 in between two molecules of **2** (1.2 kcal·mol^{-1}). This adduct yields to the side-on coordination of H_2 to one Lu^{II} center while the second Lu^{II} remains in the vicinity (+5.4 kcal·mol^{-1}). It is important to note that these two adducts do not imply oxidation of the Lu center since the most stable one is on the triplet PES and the unpaired spin density is mainly located at the two Lu centers (see Figure S46). However, the H–H distance (0.82 Å) is elongated, and the SOMO implies interaction between a d orbital on Lu^{II} and the σ* of H_2 (see Figure S47). This coordination has thus decreased the energy of the H_2 σ* orbital (which is now involved in the SOMO), allowing further reduction of H_2 *via* a bimetallic transition state (TS). At the TS, H_2 is undergoing a two-electron reduction that allows the disruption of the H–H bond with an accessible barrier of 24.2 kcal·mol^{-1}. The value for this activation barrier is fully consistent with the relatively slow reaction observed at room temperature. The TS was located on the singlet PES in line with a two-electron reduction and the need of bimetallic activation since each Lu^{II} is only able to do one single electron transfer. The H_2 molecule is becoming end-on coordinated to the Lu center (Lu–H distance of 2.20 Å) while the H–H distance is only marginally elongated with respect to the adduct (0.88 Å). The second H···Lu distance remains long (3.47 Å) but the interaction is effective, as highlighted by the HOMO at the TS (Figure 6b), where the two d_{z^2} orbitals located on the two Lu atoms overlap with the H_2 σ* orbital. Following the intrinsic reaction coordinate (IRC), it yields two Lu^{III}–H complexes whose formation is highly favorable (–36.4 kcal·mol^{-1} with respect to the entrance channel).

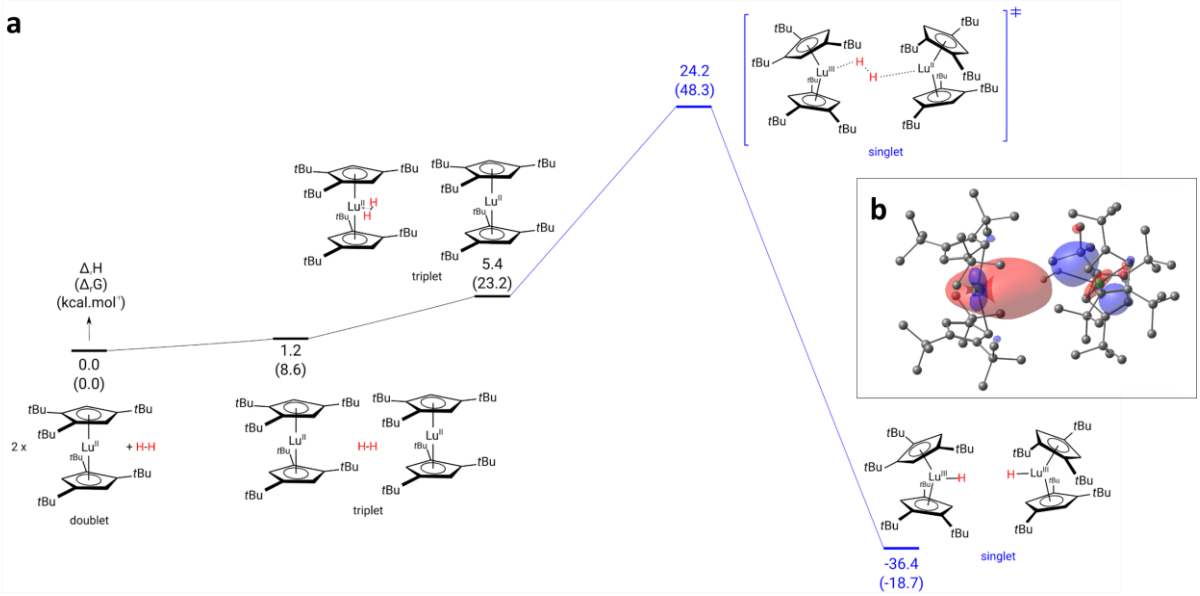

Figure 6. (a) Computed energy profile for the reaction of **2** with H_2 leading to the formation of **3-H**. (b) Calculated HOMO at the TS of the reaction between **2** and H_2 showing the two metal d_{z^2} orbitals of two molecules of **2** overlapping with the H_2 σ* orbital.

*Reactivity of **2** towards small molecules: N_2 coordination*

The exceptional sensitivity of **2** towards N_2 prompted us to examine the nature of the resulting product and study the possibility of synergistic H_2/N_2 activation reactions. The addition of N_2 to a pentane solution of **2** led to the immediate formation of a deep purple suspension of $[\{Lu(Cp^{ttt})_2\}_2(\mu\text{-}\eta^1\text{:}\eta^1\text{-}N_2)]$ (**5**) (Figure 7a). This work parallels the recent synthesis by Layfield and co-workers of the analogous Gd, Tb, and Dy complexes by *in situ* reaction of the elusive divalent complexes with N_2.[35b]

Crystals of **5** suitable of X-ray diffraction studies revealed the formation of a centrosymmetric dinuclear Lu^{III} complex featuring an end-on bridging $(N_2)^{2-}$ ligand (Figure 7b). Although N_2 coordination on low-valent RE complexes is relatively common, the end-on $\mu\text{–}\eta^1\text{:}\eta^1\text{-}N_2$ coordination mode is still rare,[35b,50] typically favored by bulky ligands and RE metals of small ionic radii. As expected from the lanthanide contraction, the Lu–N separation of 2.184(5) Å is slightly shorter than the Ln–N separations of 2.325(4), 2.296(4) and 2.268(7) Å in the Gd, Tb and Dy analogues, respectively.[35b] The N–N separation of 1.203(11) Å is consistent with a doubly reduced $(N_2)^{2-}$ ligand, which is corroborated by vibrational spectroscopy. Although the IR spectrum of **5** is very similar to that of **2** (Figure S29) because the N=N vibration is not IR active in this centrosymmetric structure, the Raman spectrum of **5** revealed a sharp band at 1610 cm^{-1} for the symmetric N_2 stretch (Figure 7e). This assignment was confirmed by the shift of this signal to 1559 cm^{-1} for the ^{15}N-labeled complex **5-^{15}N**. The experimental ratio of frequencies of 1.033 matches the theoretical value of 1.035 derived from reduced mass considerations. It is worth noting that the extent of N_2 activation in rare-earth metal diazenido complexes seems to particularly depend on the $(N_2)^{2-}$ coordination mode. For the most common side-on coordination mode, the N_2

stretch lies in the range 1371–1473 cm^{-1},[11c,51] whereas the reported N_2 stretching vibration in end-on complexes is at higher energy, ranging from 1595 to 1660 cm^{-1}.[35b,50]

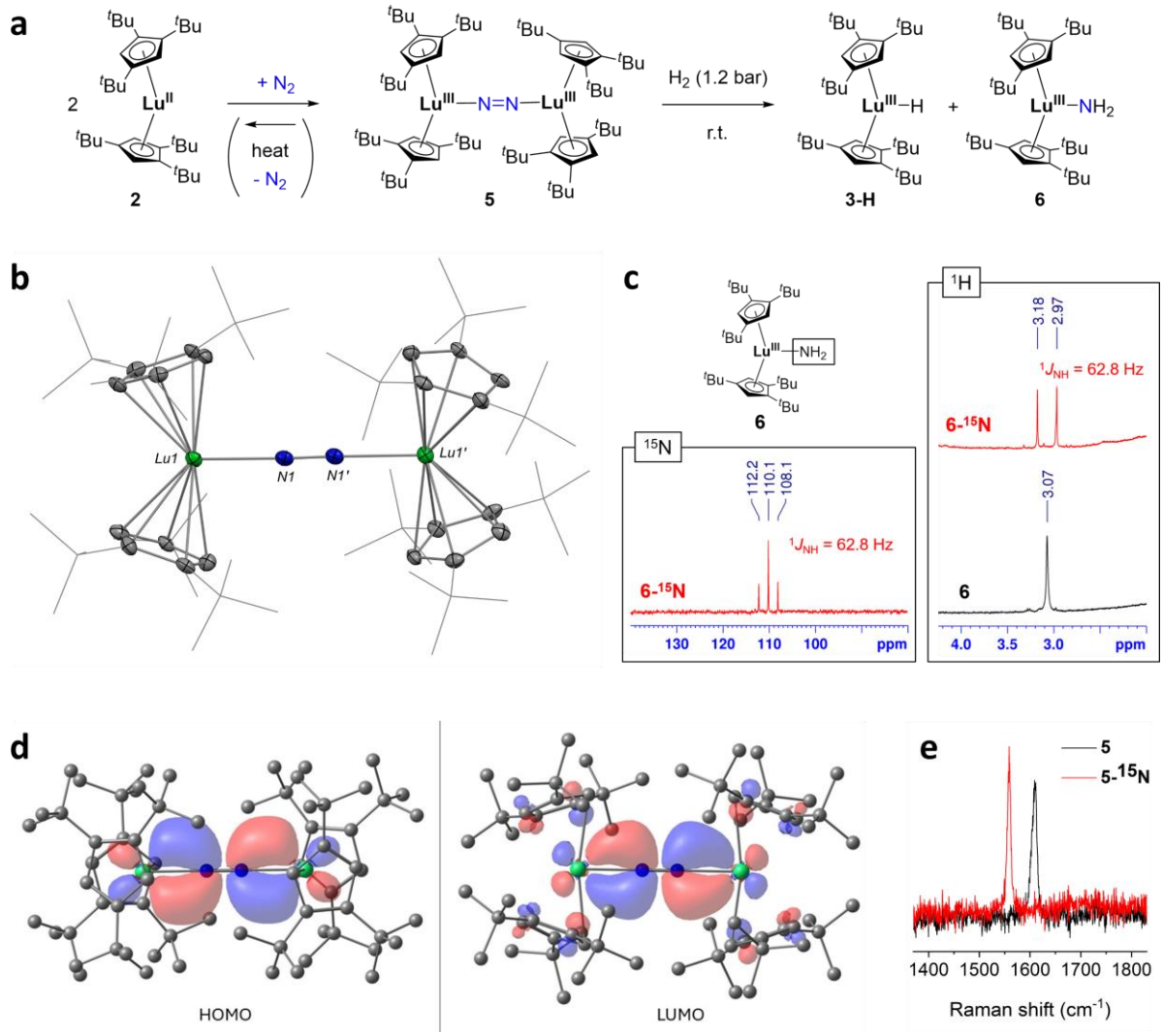

Figure 7. (a) Synthesis and hydrogenation reactivity of **5**. (b) Centrosymmetric molecular structure of **5** in the solid state with the thermal ellipsoids at the 40% probability level (except for the ^{t}Bu groups depicted in wireframe). H atoms and non-coordinating solvent molecules have been omitted for clarity. (c) Details of the NH_2 regions in the ^{1}H and ^{15}N NMR spectra of **6** and **6-^{15}N**. (d) Calculated HOMO and LUMO of **5**. (e) Raman spectrum of **5** and comparison with that of **5-^{15}N**.

Once formed, **5** is only sparingly soluble in hydrocarbon solvents and readily decomposes in ether solvents to unidentified species, which hampered analysis by NMR spectroscopy. The UV-vis spectrum in pentane of *in situ* formed **5** shows the disappearance of the characteristic band of **2** centered at 435 nm, at the expense of two intense absorption bands at 310 (ε = 5900 $L \cdot mol^{-1} \cdot cm^{-1}$) and 555 nm ($\varepsilon$ = 5300 $L \cdot mol^{-1} \cdot cm^{-1}$) (Figure 4). The latter band is slightly blue-shifted compared to that in the corresponding Dy complex, following the preliminary trend observed in the [{Ln(Cp^{ttt})$_2$}$_2$(μ-η^1:η^1-N_2)] (Ln = Gd, Tb, Dy) series.[35b]

The structure of complex **5** was investigated computationally using the same methodology as before. Both end-on and side-on coordination of N_2 were considered and the end-on coordination is found to be the most favorable. In the same way, the singlet and triplet spin states were considered for complex **5**, as a recent report by Jones and co-workers demonstrated that the $(N_2)^{2-}$ ligand can adopt a triplet ground state by occupying the two formally degenerated π^* orbital of N_2.[52] A similar triplet ground state was observed by Evans and co-workers for end-on coordinated dinitrogen Sc and Gd ion-pair complexes supported by silylamide ligands.[50a,50b] In the case of **5**, the singlet is found to be slightly more stable than the triplet by 1.8 kcal·mol^{-1}, consistent with the recent findings of Layfield and co-workers on the Gd, Tb and Dy analogues.[35b] The singlet optimized geometry compares well with the experimental one (Lu–N distance of 2.20 Å and N–N distance of 1.20 Å), in line with a two-electron reduction of N_2 upon coordination to two Lu^{II} fragments. This reduction, evidenced by the N–N distance variation, is also highlighted by the nature of the HOMO where two d_{xy} orbitals overlap with one of the N_2 π^* while the second π^* orbital overlaps with the d_{xz} in the LUMO (Figure 7d).

It should be noted that, although **2** presents a very strong affinity for dinitrogen, the N_2 coordination is reversible with temperature (Figure 7a). Upon heating a solution of **5** in tol-d_8 to reflux in a sealed NMR tube under an argon atmosphere, the purple color slowly fades away, leading to the orange-red color characteristic of **2**. Agitation of the NMR tube immediately returns the original purple colors, indicating re-coordination of the N_2 ligand. A movie about this transformation can be found in the Supporting Information section. Reversible N_2 coordination is unusual in RE dinitrogen complexes, dominated by side-on N_2 coordination. It has historically been observed in some Sm^{II} complexes,[53] which are less reducing than non-classical Ln^{II} complexes and thus afford weaker N_2 activation. In the case of RE end-on coordinated $(N_2)^{2-}$ complexes, the liberation of N_2 with concomitant generation, even transiently, of Ln^{II} species seems to be more common and has been observed both thermally[50b,50d] or under UV light irradiation.[50a]

*Reactivity of **2** towards small molecules: towards N_2 hydrogenation*

With the two components of H_2 splitting and N_2 reduction to a $(N_2)^{2-}$ in hand, we focused on their synergy in relation to N_2 hydrogenation, relevant to the Haber–Bosch process. We were interested in the reactivity of **5** towards H_2 as Ln^{III} dinitrogen complexes, which feature formally oxidized metal centers, have been shown to act as "masked" low-valent synthons.[35b,50e,54] In these examples, two-electron reduction processes occurred upon addition of reducible substrates (CO, CO_2, aromatic *N*-heterocycles), with the systematic release of the N_2 ligand. Similar reductive reactivity has also been recently reported in the case of N_2 complexes of U^{IV}, Mg^{II} and Ca^{II}, where the coordinated and reduced $(N_2)^{2-}$ moiety acted as a redox-active ligand, able to reversibly store two electrons.[52,55]

Initial reactivity attempts in NMR tubes showed that heating a purple suspension of **5** in C_6D_6 under H_2 atmosphere at 80 °C led to the full consumption of **5** over several hours, as evidenced by the

formation of a clear colorless solution. ^{1}H NMR analysis revealed the formation of **3-H** as a major product (*ca.* 90%) along with a minor species (*ca.* 10%) assigned to [Lu(Cp^{ttt})$_2$NH$_2$] (**6**) (Figure 7a). The identity of **6** was testified by ^{15}N labelling experiments as well as independent *in situ* synthesis of **6** upon exposure of **2** with NH_3 gas (Figures S15–18). In the ^{1}H NMR spectrum, the singlet at δ 3.07 ppm for the NH_2 protons in **6** was replaced by a doublet ($^{1}J_{HN}$ = 62.8 Hz) when performing the experiment with the isotopically labelled **5-^{15}N**. Accordingly, the ^{15}N NMR spectrum of **6-^{15}N** showed a triplet at δ 110.1 ppm with the same coupling constant (Figure 7c). In addition, protonolysis experiments with anhydrous HCl confirmed the formation of NH_4Cl and $^{15}NH_4Cl$, as evidenced by the presence in the ^{1}H NMR spectra of the characteristic triplet and doublet signals, respectively, in the range δ 7.2–7.7 ppm (see Figure S21). The origin of the NH_2 hydrogen atoms in **6** and **6-^{15}N** was confirmed by reaction of **5** and **5-^{15}N** with D_2, leading to the disappearance of the NH_2 resonance at δ 3.07 ppm while the signals for the Cp^{ttt} ligand remained unchanged (Figures S19–20).

As decoordination of the N_2 ligand in **5** is favored with temperature, we hypothesized that the formation of **3-H** might arise from the reaction of *in situ* liberated **2** with H_2. We reasoned that lower temperatures should be beneficial for higher conversions into **6** *vs.* **3-H**. Although the reaction appeared kinetically blocked below 0 °C, full conversion was observed upon stirring a toluene or pentane suspension of **5** under H_2 atmosphere over 1–5 days at 0 °C or room temperature. Under these conditions, **6** was consistently formed in 20–32% NMR yields (Figures S19–20).

The exact mechanism of the N_2 hydrogenation reactivity remains elusive to date but control experiments revealed no reaction between **3-H** and N_2 at different temperatures (Figure S22). Although M–NH_2 moieties have been obtained upon hydrogenation of terminal uranium or iridium nitride complexes,[56] the inaccessibility of oxidation states higher than +III for Lu would prevent the formation of a similar intermediate. As such, the formation of **6** is bound to proceed through direct hydrogenation of the N_2-ligated complex **5**, an unprecedented reactivity in RE chemistry. The observed N_2-hydrogenation reactivity is all the more remarkable as it occurs on a doubly-reduced $(N_2)^{2-}$ ligand. So far, the very rare examples of N_2-functionalization on RE complexes (Figure 1a) have systematically required further activation of the N_2 ligand *via* formation of the $(N_2)^{3-}$ radical anion.[11]

Conclusion

The present work describes the synthesis and reactivity of a rare example of Lu^{II} neutral complex. The fluxionality of the Cp^{ttt} ligand is essential to provide kinetic stabilization of the divalent metal center while still allowing coordination of exogenous ligands. The Lu^{II} complex, **2**, reduces H_2 at room temperature to give a Lu^{III}–hydride complex, which corresponds to the first example of direct H_2 splitting by a molecular rare-earth complex. This unusual reactivity has been fully supported by DFT calculations. In addition, **2** readily reacts with N_2 with reversible formation of an end-on coordinated $(N_2)^{2-}$ complex. The latter reacts with H_2 under very smooth conditions yielding a Lu^{III}–NH_2 *via* direct

hydrogenation of the reduced dinitrogen complex. This novel reactivity in RE chemistry, allowing both N≡N bond cleavage and N–H bond formation, opens new avenues for N_2 hydrogenation and functionalization using metals that have so far been neglected for such transformations.

Associated Content

- Supporting Information: Full experimental details and characterization data, NMR spectra, IR and Raman spectra, UV-vis absorption spectra, EPR spectra, X-ray crystallographic details and DFT calculation details (PDF file).
- Supplementary Data1: Crystallographic data for compounds **1**, **2**, **3-H**, **3-D** and **5** (CCDC reference 2407686-2407690) (CIF file)
- Supplementary Data2: Cartesian coordinates of all DFT computed structures (XYZ file).
- Supplementary Data3: Movie for the reversible transformation of **5** into **2** upon heating (MP4 file).

Data availability

X-ray crystallographic data for **1**, **2**, **3-H**, **3-D** and **5** are available from the Cambridge Crystallographic Data Centre (CCDC 2407686-2407690) free of charge via https://www.ccdc.cam.ac.uk/structures/.

Author Information Notes

The manuscript was written through contributions of all authors, and all authors have given approval to the final version of the manuscript.

The authors declare no competing financial interest.

ORCID ID:

- for TS: orcid.org/0000-0002-0184-303X
- for LM: orcid.org/0000-0003-2653-8557
- for GN: orcid.org/0000-0003-0599-1176

Acknowledgements

Dr. Florian Jaroschik and Dr. Grégory Danoun are thanked for fruitful discussions. CNRS and Ecole Polytechnique are thanked for funding. This research was funded, in whole or in part, by the French National Research Agency (ANR) under the project number ANR-23-CE07-0012. A CC-BY public copyright license has been applied by the authors to the present document and will be applied to all subsequent versions up to the Author Accepted Manuscript arising from this submission, in accordance with the grant's open access conditions. Parts of this work have received funding from the European Research Council (ERC) under the European Union's Horizon H2020 research program (grant

agreement no. 101044892). We acknowledge ResoMag facility (IP-Paris/CNRS) for the support with NMR facility. L.M. is a senior member of the Institut Universitaire de France. The authors acknowledge the HPCs CALcul en Midi-Pyrénées (CALMIP-EOS grant 1415).

References

(1) Castelvecchi, D. How the hydrogen revolution can help save the planet—and how it can't. *Nature* **2022**, *611*, 440-443.

(2) (a) Chen, L.; Verma, P.; Hou, K.; Qi, Z.; Zhang, S.; Liu, Y.-S.; Guo, J.; Stavila, V.; Allendorf, M. D.; Zheng, L.; Salmeron, M.; Prendergast, D.; Somorjai, G. A.; Su, J. Reversible dehydrogenation and rehydrogenation of cyclohexane and methylcyclohexane by single-site platinum catalyst. *Nat. Commun.* **2022**, *13*, 1092; (b) Allendorf, M. D.; Stavila, V.; Snider, J. L.; Witman, M.; Bowden, M. E.; Brooks, K.; Tran, B. L.; Autrey, T. Challenges to developing materials for the transport and storage of hydrogen. *Nat. Chem.* **2022**, *14*, 1214-1223.

(3) MacFarlane, D. R.; Cherepanov, P. V.; Choi, J.; Suryanto, B. H. R.; Hodgetts, R. Y.; Bakker, J. M.; Ferrero Vallana, F. M.; Simonov, A. N. A Roadmap to the Ammonia Economy. *Joule* **2020**, *4*, 1186-1205.

(4) Wong, A. Y. H.; Selin, N. E.; Eastham, S. D.; Mounaïm-Rousselle, C.; Zhang, Y.; Allroggen, F. Climate and air quality impact of using ammonia as an alternative shipping fuel. *Environ. Res. Lett.* **2024**, *19*, 084002.

(5) Smith, C.; Hill, A. K.; Torrente-Murciano, L. Current and future role of Haber–Bosch ammonia in a carbon-free energy landscape. *Energy Environ. Sci.* **2020**, *13*, 331-344.

(6) (a) Nishibayashi, Y.; Iwai, S.; Hidai, M. Bimetallic System for Nitrogen Fixation: Ruthenium-Assisted Protonation of Coordinated N_2 on Tungsten with H_2. *Science* **1998**, *279*, 540-542; (b) Pool, J. A.; Lobkovsky, E.; Chirik, P. J. Hydrogenation and cleavage of dinitrogen to ammonia with a zirconium complex. *Nature* **2004**, *427*, 527-530.

(7) (a) Onishi, N.; Laurenczy, G.; Beller, M.; Himeda, Y. Recent progress for reversible homogeneous catalytic hydrogen storage in formic acid and in methanol. *Coord. Chem. Rev.* **2018**, *373*, 317-332; (b) Kushwaha, S.; Parthiban, J.; Singh, S. K. Recent Developments in Reversible CO_2 Hydrogenation and Formic Acid Dehydrogenation over Molecular Catalysts. *ACS Omega* **2023**, *8*, 38773-38793.

(8) (a) Falcone, M.; Chatelain, L.; Scopelliti, R.; Živković, I.; Mazzanti, M. Nitrogen reduction and functionalization by a multimetallic uranium nitride complex. *Nature* **2017**, *547*, 332-335; (b) Chalkley, M. J.; Drover, M. W.; Peters, J. C. Catalytic N_2-to-NH_3 (or -N_2H_4) Conversion by Well-Defined Molecular Coordination Complexes. *Chem. Rev.* **2020**, *120*, 5582-5636; (c) Bennaamane, S.; Espada, M. F.; Mulas, A.; Personeni, T.; Saffon-Merceron, N.; Fustier-Boutignon, M.; Bucher, C.; Mézailles, N. Catalytic Reduction of N_2 to Borylamine at a Molybdenum Complex. *Angew. Chem. Int. Ed.* **2021**, *60*, 20210-20214; (d) Xin, X.; Douair, I.; Zhao, Y.; Wang, S.; Maron, L.; Zhu, C. Dinitrogen cleavage and hydrogenation to ammonia with a uranium complex. *Nat. Sci. Rev.* **2022**, *10*, nwac144; (e) Tanabe, Y.; Nishibayashi, Y. Catalytic Nitrogen Fixation Using Well-Defined Molecular Catalysts under Ambient or Mild Reaction Conditions. *Angew. Chem. Int. Ed.* **2024**, *63*, e202406404.

(9) Shima, T.; Hu, S.; Luo, G.; Kang, X.; Luo, Y.; Hou, Z. Dinitrogen Cleavage and Hydrogenation by a Trinuclear Titanium Polyhydride Complex. *Science* **2013**, *340*, 1549-1552.

(10) Reiners, M.; Baabe, D.; Münster, K.; Zaretzke, M.-K.; Freytag, M.; Jones, P. G.; Coppel, Y.; Bontemps, S.; Rosal, I. d.; Maron, L.; Walter, M. D. NH_3 formation from N_2 and H_2 mediated by molecular tri-iron complexes. *Nat. Chem.* **2020**, *12*, 740-746.

(11) (a) Fang, M.; Lee, D. S.; Ziller, J. W.; Doedens, R. J.; Bates, J. E.; Furche, F.; Evans, W. J. Synthesis of the $(N_2)^{3-}$ Radical from Y^{2+} and Its Protonolysis Reactivity To Form $(N_2H_2)^{2-}$ via the $Y[N(SiMe_3)_2]_3/KC_8$ Reduction System. *J. Am. Chem. Soc.* **2011**, *133*, 3784-3787; (b) Lv, Z.-J.; Huang, Z.; Zhang, W.-X.; Xi, Z.

Scandium-Promoted Direct Conversion of Dinitrogen into Hydrazine Derivatives via N–C Bond Formation. *J. Am. Chem. Soc.* **2019**, *141*, 8773-8777; (c) Chen, X.; Wang, G.-X.; Lv, Z.-J.; Wei, J.; Xi, Z. Monomethylation and -protonation of Lutetium Dinitrogen Complex. *J. Am. Chem. Soc.* **2024**, *146*, 17624-17628; (d) Shivaraam, R. A. K.; Rajeshkumar, T.; Scopelliti, R.; Živković, I.; Maron, L.; Mazzanti, M. Dinitrogen Reduction and Functionalization by a Siloxide Supported Thulium-Potassium Complex for the formation of Ammonia or Hydrazine Derivatives. *Angew. Chem. Int. Ed.* **2024**, *n/a*, ASAP e202414051.

(12) Wong, A.; Lam, F. Y. T.; Hernandez, M.; Lara, J.; Trinh, T. M.; Kelly, R. P.; Ochiai, T.; Rao, G.; Britt, R. D.; Kaltsoyannis, N.; Arnold, P. L. Catalytic reduction of dinitrogen to silylamines by earth-abundant lanthanide and group 4 complexes. *Chem Catal.* **2024**, *4*, 100964.

(13) (a) Kim, S.; Park, Y.; Kim, J.; Pabst, T. P.; Chirik, P. J. Ammonia synthesis by photocatalytic hydrogenation of a N_2-derived molybdenum nitride. *Nat. Synth.* **2022**, *1*, 297-303; (b) Johansen, C. M.; Boyd, E. A.; Peters, J. C. Catalytic transfer hydrogenation of N_2 to NH_3 *via* a photoredox catalysis strategy. *Sci. Adv.* **2022**, *8*, eade3510; (c) Ashida, Y.; Onozuka, Y.; Arashiba, K.; Konomi, A.; Tanaka, H.; Kuriyama, S.; Yamazaki, Y.; Yoshizawa, K.; Nishibayashi, Y. Catalytic nitrogen fixation using visible light energy. *Nat. Commun.* **2022**, *13*, 7263.

(14) Bhimpuria, R.; Thapper, A.; Borbas, K. E. Sm(II)-catalyzed reduction of dinitrogen, nitrite and nitrate to ammonia or urea. *ChemRxiv* **2024**, doi: 10.26434/chemrxiv-2024-35sv7 This content is a preprint and has not been peer-reviewed.

(15) Cotton, S. In *Lanthanide and Actinide Chemistry*; John Wiley & Sons, Ltd.: Chichester (U.K.), 2006, p. 1-263.

(16) (a) Mahieu, N.; Piątkowski, J.; Simler, T.; Nocton, G. Back to the future of organolanthanide chemistry. *Chem. Sci.* **2023**, *14*, 443-457; (b) Schäfer, S.; Kaufmann, S.; Rösch, E. S.; Roesky, P. W. Divalent metallocenes of the lanthanides – a guideline to properties and reactivity. *Chem. Soc. Rev.* **2023**, *52*, 4006-4045.

(17) (a) Evans, W. J. Tutorial on the Role of Cyclopentadienyl Ligands in the Discovery of Molecular Complexes of the Rare-Earth and Actinide Metals in New Oxidation States. *Organometallics* **2016**, *35*, 3088-3100; (b) Gould, C. A.; McClain, K. R.; Yu, J. M.; Groshens, T. J.; Furche, F.; Harvey, B. G.; Long, J. R. Synthesis and Magnetism of Neutral, Linear Metallocene Complexes of Terbium(II) and Dysprosium(II). *J. Am. Chem. Soc.* **2019**, *141*, 12967-12973; (c) Wedal, J. C.; Evans, W. J. A Rare-Earth Metal Retrospective to Stimulate All Fields. *J. Am. Chem. Soc.* **2021**, *143*, 18354-18367; (d) McClain, K. R.; Gould, C. A.; Marchiori, D. A.; Kwon, H.; Nguyen, T. T.; Rosenkoetter, K. E.; Kuzmina, D.; Tuna, F.; Britt, R. D.; Long, J. R.; Harvey, B. G. Divalent Lanthanide Metallocene Complexes with a Linear Coordination Geometry and Pronounced 6s–5d Orbital Mixing. *J. Am. Chem. Soc.* **2022**, *144*, 22193-22201.

(18) Nief, F. Non-classical divalent lanthanide complexes. *Dalton Trans.* **2010**, *39*, 6589-6598.

(19) Trinh, M. T.; Wedal, J. C.; Evans, W. J. Evaluating electrochemical accessibility of $4f^n5d^1$ and $4f^{n+1}$ Ln(II) ions in $(C_5H_4SiMe_3)_3Ln$ and $(C_5Me_4H)_3Ln$ complexes. *Dalton Trans.* **2021**, *50*, 14384-14389.

(20) (a) Evans, W. J.; Allen, N. T.; Ziller, J. W. Facile Dinitrogen Reduction via Organometallic Tm(II) Chemistry. *J. Am. Chem. Soc.* **2001**, *123*, 7927-7928; (b) Bochkarev, M. N.; Khoroshenkov, G. V.; Schumann, H.; Dechert, S. A Novel Bis(imino)amine Ligand as a Result of Acetonitrile Coupling with the Diiodides of Dy(II) and Tm(II). *J. Am. Chem. Soc.* **2003**, *125*, 2894-2895; (c) Jaroschik, F.; Nief, F.; Le Goff, X.-F.; Ricard, L. Synthesis and Reactivity of Organometallic Complexes of Divalent Thulium with Cyclopentadienyl and Phospholyl Ligands. *Organometallics* **2007**, *26*, 3552-3558; (d) Nocton, G.; Ricard, L. Reversible C–C coupling in phenanthroline complexes of divalent samarium and thulium. *Chem. Commun.* **2015**, *51*, 3578-3581; (e) Ryan, A. J.; Ziller, J. W.; Evans, W. J. The importance of the counter-cation in reductive rare-earth metal chemistry: 18-crown-6 instead of 2,2,2-cryptand allows isolation of $[Y^{II}(NR_2)_3]^{1-}$ and ynediolate and enediolate complexes from CO reactions. *Chem. Sci.* **2020**, *11*, 2006-2014; (f) Demkin, A. G.; Savkov, B. Y.; Sukhikh, T. S.; Konchenko, S. N. First examples of molecular polychalcogenide complexes of thulium. *J. Struct. Chem.* **2021**, *62*, 957-965; (g) Dodonov, V. A.; Makarov, V. M.; Zemnyukova, M. N.; Razborov, D. A.; Baranov, E. V.; Bogomyakov, A. S.; Ovcharenko, V. I.;

Fedushkin, I. L. Stability and Solution Behavior of [(dpp-Bian)Ln] and [(dpp-Bian)LnX] (Ln = Yb, Tm, or Dy; X = I, F, or N_3). *Organometallics* **2023**, *42*, 2558-2567.

(21) Simler, T.; McCabe, K. N.; Maron, L.; Nocton, G. CO reductive oligomerization by a divalent thulium complex and CO_2-induced functionalization. *Chem. Sci.* **2022**, *13*, 7449-7461.

(22) Weber, F.; Schultz, M.; Sofield, C. D.; Andersen, R. A. Synthesis and Solid State Structures of Sterically Crowded d^0-Metallocenes of Magnesium, Calcium, Strontium, Barium, Samarium, and Ytterbium. *Organometallics* **2002**, *21*, 3139-3146.

(23) (a) Evans, W. J.; Allen, N. T.; Ziller, J. W. Expanding Divalent Organolanthanide Chemistry: The First Organothulium(II) Complex and the In Situ Organodysprosium(II) Reduction of Dinitrogen. *Angew. Chem. Int. Ed.* **2002**, *41*, 359-361; (b) Nief, F.; de Borms, B. T.; Ricard, L.; Carmichael, D. New Complexes of Divalent Thulium with Substituted Phospholyl and Cyclopentadienyl Ligands. *Eur. J. Inorg. Chem.* **2005**, *2005*, 637-643.

(24) Kundu, K.; White, J. R. K.; Moehring, S. A.; Yu, J. M.; Ziller, J. W.; Furche, F.; Evans, W. J.; Hill, S. A 9.2-GHz clock transition in a Lu(II) molecular spin qubit arising from a 3,467-MHz hyperfine interaction. *Nat. Chem.* **2022**, *14*, 392-397.

(25) MacDonald, M. R.; Bates, J. E.; Ziller, J. W.; Furche, F.; Evans, W. J. Completing the Series of +2 Ions for the Lanthanide Elements: Synthesis of Molecular Complexes of Pr^{2+}, Gd^{2+}, Tb^{2+}, and Lu^{2+}. *J. Am. Chem. Soc.* **2013**, *135*, 9857-9868.

(26) Anderson-Sanchez, L. M.; Yu, J. M.; Ziller, J. W.; Furche, F.; Evans, W. J. Room-Temperature Stable Ln(II) Complexes Supported by 2,6-Diadamantyl Aryloxide Ligands. *Inorg. Chem.* **2023**, *62*, 706-714.

(27) (a) Queen, J. D.; Anderson-Sanchez, L. M.; Stennett, C. R.; Rajabi, A.; Ziller, J. W.; Furche, F.; Evans, W. J. Synthesis of Crystallographically Characterizable Bis(cyclopentadienyl) Sc(II) Complexes: $(C_5H_2{}^tBu_3)_2Sc$ and $\{[C_5H_3(SiMe_3)_2]_2ScI\}^{1-}$. *J. Am. Chem. Soc.* **2024**, *146*, 3279-3292; (b) Queen, J. D.; Goudzwaard, Q. E.; Rajabi, A.; Ziller, J. W.; Furche, F.; Evans, W. J. The Scandium(II) Carbonyl Complex $(C_5H_2{}^tBu_3)_2Sc(CO)$ and its Isocyanide Analog $(C_5H_2{}^tBu_3)_2Sc(CNC_6H_3Me_2\text{-}2,6)$. *J. Am. Chem. Soc.* **2024**, *146*, 24770-24775.

(28) Ortu, F. Rare Earth Starting Materials and Methodologies for Synthetic Chemistry. *Chem. Rev.* **2022**, *122*, 6040-6116.

(29) Jaroschik, F.; Nief, F.; Le Goff, X.-F.; Ricard, L. Isolation of Stable Organodysprosium(II) Complexes by Chemical Reduction of Dysprosium(III) Precursors. *Organometallics* **2007**, *26*, 1123-1125.

(30) (a) Goodwin, C. A. P.; Reta, D.; Ortu, F.; Liu, J.; Chilton, N. F.; Mills, D. P. Terbocenium: completing a heavy lanthanide metallocenium cation family with an alternative anion abstraction strategy. *Chem. Commun.* **2018**, *54*, 9182-9185; (b) Ortu, F.; Packer, D.; Liu, J.; Burton, M.; Formanuik, A.; Mills, D. P. Synthesis and structural characterization of lanthanum and cerium substituted cyclopentadienyl borohydride complexes. *J. Organomet. Chem.* **2018**, *857*, 45-51.

(31) Price, C. G. T.; Mondal, A.; Durrant, J. P.; Tang, J.; Layfield, R. A. Structural and Magnetization Dynamics of Borohydride-Bridged Rare-Earth Metallocenium Cations. *Inorg. Chem.* **2023**, *62*, 9924-9933.

(32) Shannon, R. Revised effective ionic radii and systematic studies of interatomic distances in halides and chalcogenides. *Acta Crystallogr., Sect. A* **1976**, *32*, 751-767.

(33) (a) Marks, T. J.; Kolb, J. R. Covalent transition metal, lanthanide, and actinide tetrahydroborate complexes. *Chem. Rev.* **1977**, *77*, 263-293; (b) Ephritikhine, M. Synthesis, Structure, and Reactions of Hydride, Borohydride, and Aluminohydride Compounds of the f-Elements. *Chem. Rev.* **1997**, *97*, 2193-2242; (c) Visseaux, M.; Bonnet, F. Borohydride complexes of rare earths, and their applications in various organic transformations. *Coord. Chem. Rev.* **2011**, *255*, 374-420.

(34) (a) Schumann, H.; Genthe, W. Metallorganische Verbindungen der Lanthanoide: XI. Dicyclopentadienyllutetiumhydrid. *J. Organomet. Chem.* **1981**, *213*, C7-C9; (b) Schumann, H.; Genthe,

W.; Bruncks, N.; Pickardt, J. Organometallic compounds of the lanthanides. 15. Synthesis and x-ray crystal structure of monomeric alkyldicyclopentadienyllanthanide compounds. *Organometallics* **1982**, *1*, 1194-1200.

(35) (a) Jaroschik, F.; Nief, F.; Ricard, L. Synthesis of a new stable, neutral organothulium(II) complex by reduction of a thulium(III) precursor. *Chem. Commun.* **2006**, 426-428; (b) Mondal, A.; Price, C. G. T.; Tang, J.; Layfield, R. A. Targeted Synthesis of End-On Dinitrogen-Bridged Lanthanide Metallocenes and Their Reactivity as Divalent Synthons. *J. Am. Chem. Soc.* **2023**, *145*, 20121-20131.

(36) Guzei, I. A.; Wendt, M. An improved method for the computation of ligand steric effects based on solid angles. *Dalton Trans.* **2006**, 3991-3999.

(37) (a) Quadrelli, E. A. Lanthanide Contraction over the 4f Series Follows a Quadratic Decay. *Inorg. Chem.* **2002**, *41*, 167-169; (b) Seitz, M.; Oliver, A. G.; Raymond, K. N. The Lanthanide Contraction Revisited. *J. Am. Chem. Soc.* **2007**, *129*, 11153-11160; (c) Jordan, R. B. Lanthanide Contraction: What is Normal? *Inorg. Chem.* **2023**, *62*, 3715-3721.

(38) Fieser, M. E.; MacDonald, M. R.; Krull, B. T.; Bates, J. E.; Ziller, J. W.; Furche, F.; Evans, W. J. Structural, Spectroscopic, and Theoretical Comparison of Traditional vs Recently Discovered Ln^{2+} Ions in the [K(2.2.2-cryptand)][$(C_5H_4SiMe_3)_3Ln$] Complexes: The Variable Nature of Dy^{2+} and Nd^{2+}. *J. Am. Chem. Soc.* **2015**, *137*, 369-382.

(39) (a) Werkema, E. L.; Maron, L.; Eisenstein, O.; Andersen, R. A. Reactions of Monomeric [1,2,4-$(Me_3C)_3C_5H_2]_2$CeH and CO with or without H_2: An Experimental and Computational Study. *J. Am. Chem. Soc.* **2007**, *129*, 2529-2541; (b) Nocton, G.; Ricard, L. N-aromatic heterocycle adducts of bulky [1,2,4-$(Me_3C)_3C_5H_2]_2$Sm: synthesis, structure and solution analysis. *Dalton Trans.* **2014**, *43*, 4380-4387.

(40) Maron, L.; Werkema, E. L.; Perrin, L.; Eisenstein, O.; Andersen, R. A. Hydrogen for Fluorine Exchange in C_6F_6 and C_6F_5H by Monomeric [1,3,4-$(Me_3C)_3C_5H_2]_2$CeH: Experimental and Computational Studies. *J. Am. Chem. Soc.* **2005**, *127*, 279-292.

(41) Perrin, L.; Maron, L.; Eisenstein, O.; Schwartz, D. J.; Burns, C. J.; Andersen, R. A. Bonding of H_2, N_2, Ethylene, and Acetylene to Bivalent Lanthanide Metallocenes: Trends from DFT Calculations on Cp_2M and Cp^*_2M (M = Sm, Eu, Yb) and Experiments with Cp^*_2Yb. *Organometallics* **2003**, *22*, 5447-5453.

(42) Drummond Turnbull, R.; Bell, N. L. f-Block hydride complexes – synthesis, structure and reactivity. *Dalton Trans.* **2024**, *53*, 12814-12836.

(43) (a) Schumann, H.; Genthe, W.; Hahn, E.; Hossain, M. B.; Van Der Helm, D. Metallorganische Verbindungen der Lanthanoide: XXXI. Synthese und Molekülstruktur einiger Cyclopentadienyllutetiumhydride. *J. Organomet. Chem.* **1986**, *299*, 67-84; (b) Changtao, Q.; Daoli, D.; Chaozhou, N.; Zhiming, Z. Studies on organolanthanide complexes. XI. Preparation of dimeric dicyclopentadienyllutetium hydride by reduction of dicyclopentadienyl lutetium chloride with sodium hydride; its X-ray crystal structure and reactivity. *Inorg. Chim. Acta* **1988**, *146*, 129-133; (c) Knjazhanskij, S. Y.; Bulychev, B. M.; Kireeva, O. K.; Belsky, V. K.; Soloveichik, G. L. A change of the bonding mode of the alumohydride group in byscyclopentadienylhydrido REM complexes: from heterometallic to homometallic hydrides. Crystal and molecular structures of $[(\eta^5\text{-}C_5H_5)_2YB(\mu_2\text{-}H)AlH_2{\cdot}N(C_2H_5)_3]_2{\cdot}C_6H_6$, $[(\eta^5\text{-}C_5H_5)_2Lu(\mu_2\text{-}H)_2AlH{\cdot}N(C_2H_5)_3]_2{\cdot}C_6H_6$ and $[(\eta^5\text{-}C_5H_5)_2Lu]_3(\mu_2\text{-}H)_2(\mu_3\text{-}H)$. *J. Organomet. Chem.* **1991**, *414*, 11-22; (d) Takenaka, Y.; Hou, Z. Lanthanide Terminal Hydride Complexes Bearing Two Sterically Demanding $C_5Me_4SiMe_3$ Ligands. Synthesis, Structure, and Reactivity. *Organometallics* **2009**, *28*, 5196-5203.

(44) Guan, Y.; Lu, E.; Xu, X. Rare-earth mediated dihydrogen activation and catalytic hydrogenation. *J. Rare Earths* **2021**, *39*, 1017-1023.

(45) (a) Shen, O.; Chen, W. Q.; Jin, Y. T.; Shan, C. J. Syntheses and molecular structures of organolanthanoids. *Pure Appl. Chem.* **1988**, *60*, 1251-1256; (b) Dubé, T.; Conoci, S.; Gambarotta, S.; Yap, G. P. A.; Vasapollo, G. Tetrametallic Reduction of Dinitrogen: Formation of a Tetranuclear Samarium Dinitrogen Complex. *Angew. Chem. Int. Ed.* **1999**, *38*, 3657-3659; (c) Gun'ko, Y. K.; Hitchcock, P. B.; Lappert, M. F. Nonclassical Organolanthanoid Metal Chemistry: [K([18]-crown-6)(η^2-PhMe)$_2$]X (X =

[(LnCp^{t3})$_2$(μ-H)], [(LnCp''$_2$)$_2$(μ-η^6:η^6-PhMe)]) from [LnCpx$_3$], K, and [18]-crown-6 in Toluene (Ln = La, Ce; Cp^t = η^5-C$_5$H$_4$SiMe$_2$Bu^t; Cp'' = η^5-C$_5$H$_3$(SiMe$_3$)$_2$-1,3). *Organometallics* **2000**, *19*, 2832-2834; (d) Zhang, J.; Yi, W.; Zhang, Z.; Chen, Z.; Zhou, X. Facile Synthesis of Organolanthanide Hydrides with Metallic Potassium: Crystal Structures and Reactivity. *Organometallics* **2011**, *30*, 4320-4324; (e) Huang, W.; Dulong, F.; Khan, S. I.; Cantat, T.; Diaconescu, P. L. Bimetallic Cleavage of Aromatic C–H Bonds by Rare-Earth-Metal Complexes. *J. Am. Chem. Soc.* **2014**, *136*, 17410-17413; (f) Fieser, M. E.; Palumbo, C. T.; La Pierre, H. S.; Halter, D. P.; Voora, V. K.; Ziller, J. W.; Furche, F.; Meyer, K.; Evans, W. J. Comparisons of lanthanide/actinide +2 ions in a tris(aryloxide)arene coordination environment. *Chem. Sci.* **2017**, *8*, 7424-7433; (g) Huh, D. N.; Darago, L. E.; Ziller, J. W.; Evans, W. J. Utility of Lithium in Rare-Earth Metal Reduction Reactions to Form Nontraditional Ln^{2+} Complexes and Unusual [Li(2.2.2-cryptand)]$^{1+}$ Cations. *Inorg. Chem.* **2018**, *57*, 2096-2102.

(46) Nolan, S. P.; Marks, T. J. Spectroscopic detection of organolanthanide dihydrogen and olefin complexes. *J. Am. Chem. Soc.* **1989**, *111*, 8538-8540.

(47) Brackbill, I. J.; Rajeshkumar, T.; Maron, L.; Bergman, R. G.; Arnold, J. Spectroscopic and Computational Evidence of Uranium Dihydrogen Complexes. *J. Am. Chem. Soc.* **2024**, *146*, 1257-1261.

(48) Yao, X.; Ji, Y.; Huang, Z.-Q.; Zhao, Z.; Gao, P.; Guo, M.; Liu, X.; Meng, C.; Fu, Q.; Chang, C.-R.; Bao, X.; Hou, G. Nondissociative Activated Dihydrogen Binding on CeO_2 Revealed by High-Pressure Operando Solid-State NMR Spectroscopy. *J. Am. Chem. Soc.* **2024**, *146*, 24609-24618.

(49) (a) MacDonald, M. R.; Fieser, M. E.; Bates, J. E.; Ziller, J. W.; Furche, F.; Evans, W. J. Identification of the +2 Oxidation State for Uranium in a Crystalline Molecular Complex, [K(2.2.2-Cryptand)][(C$_5$H$_4$SiMe$_3$)$_3$U]. *J. Am. Chem. Soc.* **2013**, *135*, 13310-13313; (b) Langeslay, R. R.; Fieser, M. E.; Ziller, J. W.; Furche, F.; Evans, W. J. Expanding Thorium Hydride Chemistry Through Th^{2+}, Including the Synthesis of a Mixed-Valent Th^{4+}/Th^{3+} Hydride Complex. *J. Am. Chem. Soc.* **2016**, *138*, 4036-4045; (c) Windorff, C. J.; MacDonald, M. R.; Meihaus, K. R.; Ziller, J. W.; Long, J. R.; Evans, W. J. Expanding the Chemistry of Molecular U^{2+} Complexes: Synthesis, Characterization, and Reactivity of the {[C$_5$H$_3$(SiMe$_3$)$_2$]$_3$U}$^-$ Anion. *Chem.—Eur. J.* **2016**, *22*, 772-782.

(50) (a) Woen, D. H.; Chen, G. P.; Ziller, J. W.; Boyle, T. J.; Furche, F.; Evans, W. J. End-On Bridging Dinitrogen Complex of Scandium. *J. Am. Chem. Soc.* **2017**, *139*, 14861-14864; (b) Ryan, A. J.; Balasubramani, S. g.; Ziller, J. W.; Furche, F.; Evans, W. J. Formation of the End-on Bound Lanthanide Dinitrogen Complexes [(R$_2$N)$_3$Ln–N═N–Ln(NR$_2$)$_3$]$^{2-}$ from Divalent [(R$_2$N)$_3$Ln]$^{1-}$ Salts (R = SiMe$_3$). *J. Am. Chem. Soc.* **2020**, *142*, 9302-9313; (c) Chung, A. B.; Rappoport, D.; Ziller, J. W.; Cramer, R. E.; Furche, F.; Evans, W. J. Solid-State End-On to Side-On Isomerization of (N═N)$^{2-}$ in {[(R$_2$N)$_3$Nd]$_2$N$_2$}$^{2-}$ (R = SiMe$_3$) Connects *In Situ* Ln^{III}(NR$_2$)$_3$/K and Isolated [Ln^{II}(NR$_2$)$_3$]$^{1-}$ Dinitrogen Reduction. *J. Am. Chem. Soc.* **2022**, *144*, 17064-17074; (d) Queen, J. D.; Rajabi, A.; Goudzwaard, Q. E.; Yuan, Q.; Nguyen, D. K.; Ziller, J. W.; Furche, F.; Xi, Z.; Evans, W. J. Dinitrogen reduction chemistry with scandium provides a complex with two side-on (N=N)$^{2-}$ ligands bound to one metal: (C$_5$Me$_5$)Sc[(μ-η^2:η^2-N$_2$)Sc(C$_5$Me$_5$)$_2$]$_2$. *Chem. Sci.* **2024**, *15*, 16069-16078; (e) Yuan, M.; McNeece, A. J.; Dolgopolova, E. A.; Wolfsberg, L.; Bowes, E. G.; Batista, E. R.; Yang, P.; Filatov, A.; Davis, B. L. Photoinduced Isomerization of [N$_2$]$^{2-}$ in a Bimetallic Lutetium Complex. *J. Am. Chem. Soc.* **2024**, *146*, 31074-31084.

(51) (a) Fieser, M. E.; Woen, D. H.; Corbey, J. F.; Mueller, T. J.; Ziller, J. W.; Evans, W. J. Raman spectroscopy of the N–N bond in rare earth dinitrogen complexes. *Dalton Trans.* **2016**, *45*, 14634-14644; (b) Singh, D.; Buratto, W. R.; Torres, J. F.; Murray, L. J. Activation of Dinitrogen by Polynuclear Metal Complexes. *Chem. Rev.* **2020**, *120*, 5517-5581.

(52) Mondal, R.; Evans, M. J.; Rajeshkumar, T.; Maron, L.; Jones, C. Coordination and Activation of N_2 at Low-Valent Magnesium using a Heterobimetallic Approach: Synthesis and Reactivity of a Masked Dimagnesium Diradical. *Angew. Chem. Int. Ed.* **2023**, *62*, e202308347.

(53) (a) Evans, W. J.; Ulibarri, T. A.; Ziller, J. W. Isolation and X-ray crystal structure of the first dinitrogen complex of an f-element metal, [(C$_5$Me$_5$)$_2$Sm]$_2$N$_2$. *J. Am. Chem. Soc.* **1988**, *110*, 6877-6879; (b) Guan, J.; Dubé, T.; Gambarotta, S.; Yap, G. P. A. Dinitrogen Labile Coordination versus Four-Electron Reduction,

THF Cleavage, and Fragmentation Promoted by a (calix-tetrapyrrole)Sm(II) Complex. *Organometallics* **2000**, *19*, 4820-4827.

(54) (a) Evans, W. J.; Lee, D. S.; Ziller, J. W.; Kaltsoyannis, N. Trivalent $[(C_5Me_5)_2(THF)Ln]_2(\mu\text{-}\eta^2\text{:}\eta^2\text{-}N_2)$ Complexes as Reducing Agents Including the Reductive Homologation of CO to a Ketene Carboxylate, $(\mu\text{-}\eta^4\text{-}O_2CCCO)^{2-}$. *J. Am. Chem. Soc.* **2006**, *128*, 14176-14184; (b) Evans, W. J.; Lorenz, S. E.; Ziller, J. W. Investigating Metal Size Effects in the $Ln_2(\mu\text{-}\eta^2\text{:}\eta^2\text{-}N_2)$ Reduction System: Reductive Reactivity with Complexes of the Largest and Smallest Trivalent Lanthanide Ions, La^{3+} and Lu^{3+}. *Inorg. Chem.* **2009**, *48*, 2001-2009.

(55) (a) Mansell, S. M.; Kaltsoyannis, N.; Arnold, P. L. Small Molecule Activation by Uranium Tris(aryloxides): Experimental and Computational Studies of Binding of N_2, Coupling of CO, and Deoxygenation Insertion of CO_2 under Ambient Conditions. *J. Am. Chem. Soc.* **2011**, *133*, 9036-9051; (b) Evans, M. J.; Mullins, J.; Mondal, R.; Jones, C. Reductions of Arenes using a Magnesium-Dinitrogen Complex. *Chem.—Eur. J.* **2024**, *30*, e202401005; (c) Rösch, B.; Gentner, T. X.; Langer, J.; Färber, C.; Eyselein, J.; Zhao, L.; Ding, C.; Frenking, G.; Harder, S. Dinitrogen complexation and reduction at low-valent calcium. *Science* **2021**, *371*, 1125-1128.

(56) (a) Schöffel, J.; Rogachev, A. Y.; DeBeer George, S.; Burger, P. Isolation and Hydrogenation of a Complex with a Terminal Iridium–Nitrido Bond. *Angew. Chem. Int. Ed.* **2009**, *48*, 4734-4738; (b) Chatelain, L.; Louyriac, E.; Douair, I.; Lu, E.; Tuna, F.; Wooles, A. J.; Gardner, B. M.; Maron, L.; Liddle, S. T. Terminal uranium(V)-nitride hydrogenations involving direct addition or Frustrated Lewis Pair mechanisms. *Nat. Commun.* **2020**, *11*, 337.

For Table of Contents Only